Contents

PERFORMANCE ANALYSIS OF CONSTANT SPEED LOCAL OBSTACLE AVOIDANCE CONTROLLER USING AN MPC ALGORITHM ON GRANULAR TERRAIN

Nicholas Haraus
Dept. of Mechanical Engineering
Marquette University
Milwaukee, WI

Radu Serban
Dept. of Mechanical Engineering
University of Wisconsin - Madison
Madison, WI

Jonathan Fleischmann
Dept. of Mechanical Engineering
Marquette University
Milwaukee, WI

ABSTRACT

A Model Predictive Control (MPC) Algorithm was used by Liu, Ersal, Stein, and Jayakumar [1] to develop a LIDAR-based constant speed local obstacle avoidance controller for autonomous ground vehicles. When provided with LIDAR data as well as a target location, a vehicle can route itself around obstacles as it encounters them and arrive at an end goal via an optimal route. Using Chrono, a multibody physics API, this controller has been tested on a complex multibody physics HMMWV model to perform higher fidelity testing in more situations than previously accomplished. For this research, the LIDAR-based constant speed local obstacle avoidance controller [1] has been implemented and tested on rigid flat terrain and granular terrain to examine the robustness of this control method. A novel simulation framework has been developed to efficiently simulate granular terrain for this application.

1 INTRODUCTION

s:introduction

Obstacle avoidance is a crucial capability for Autonomous Ground Vehicles (AGVs) of the future. This refers to a ground vehicles ability to sense its surrounding environment, develop an optimal path around the obstacles in the environment, generate optimal control commands to satisfy that path, and physically navigate the vehicle around the obstacles safely and to a desired endpoint. Safety is defined as avoiding collisions as well as enforcing limitations on excessive sideslip or tire lift-off. An ideal control algorithm is one that is capable of pushing a vehicle to its performance limits by using knowledge of its dynamic capabilities and surrounding environmental conditions while still enforcing the strict safety requirements. Though previous work has been accomplished testing a Model Predictive Control (MPC) algorithm for obstacle avoidance on wheeled vehicles, more work is re-

quired to test the fidelity of this algorithm and determine where improvements are needed. One area in which this algorithm has yet to be tested is its ability to control a wheeled vehicle on deformable terrain. Up to this point, the assumption that the terrain is rigid and flat for testing has been used. However, when rigid terrain is replaced with deformable terrain, such as soil or sand, how does the MPC algorithm perform? Do the current most commonly used vehicle models perform successfully with the MPC algorithm on deformable terrain? The proposed research evaluates the robustness and validity of the MPC algorithm with different vehicle models in an environment more similar to what an off-road military vehicle would experience in combat. This testing is done via numerical simulation.

The goal of this paper is to present the results of this study to understand how model fidelity of the controller model affects overall performance of the obstacle avoidance controller. Certain challenges are introduced when attempting to simulate a vehicle on granular terrain: Specifically, how does the user efficiently allow the vehicle to drive everywhere without creating billions of particles scattered across the entire terrain? This challenge has been addressed by employing a simulation framework for granular terrain developed by the authors. The study has the following three objectives:

1. Study and compare the performance of the MPC Controller on granular terrain compared to rigid terrain.

2. Analyze the role of model fidelity of the internal controller model and how it affects the speed and performance of the obstacle avoidance controller.

3. Showcase the potential of controller testing in a high fidelity virtual test environment with Chrono to assist with initial control algorithm development before physical implementation for vehicular applications.

The remainder of this paper is organized as follows. In Section 2 we provide overviews of the MPC based local obstacle avoidance algorithm, the Chrono multiphysics package used as the test environment. In Section 3 we describe the Chrono::Vehicle HMMWV vehicle model used in this study as the plant model to be controlled and our proposed method for simulating a vehicle driving on deformable terrain over large distances. Then, the specific MPC LIDAR based local obstacle avoidance controller used for this study is presented. We introduce the different simplified lower fidelity analytical vehicle models used in the MPC algorithm to predict the /CHRONO vehicle behavior. We also provide descriptions of the test cases run for this study and a summary of the metrics used to compare performance of the various tested combinations. In Section 4 we presents the results of the tests outlined in the previous section as well as perform appropriate comparisons of the tests when the internal controller vehicle model is varied and when the terrain is changed from rigid to granular. Section 5 wraps up the paper and presents potential future work based on the results of this study.

2 BACKGROUND

s:background

2.1 MPC Based Local Obstacle Avoidance

MPC

The concept of MPC is to use an internal model of the system one desires to control to predict and optimize future system behavior from the current system state and inputs. The system behavior is predicted over some defined finite time horizon and the optimal control sequence over the prediction horizon is output. The control sequence is executed for an execution time smaller than the prediction horizon, and the whole process is repeated. The repetition of this process over time creates a feedback loop which continually controls the system, pushing it towards an optimal path.
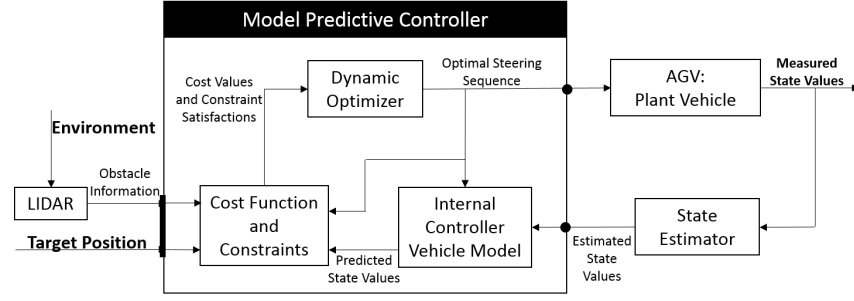
Figure 1: Schematic of MPC LIDAR-Based Constant Speed Local Obstacle Avoidance Controller

fig:MPC_schematic

For this study, the system to be controlled is an AGV. Consider an AGV located in a level environment without roads or any other structures to guide the AGVs motion. The AGV also has a known global target position. Between the target position and the current vehicle position there may or may not be obstacles of unknown size. Using the MPC formulation outlined in [1], the vehicle can navigate from the current position to the provided target position while avoiding obstacles as they are encountered. Obstacle information is assumed to be unknown a priori and only obtained through a planar LIDAR sensor. The MPC schematic is presented in Fig. 1.

ModelFidelity2016

fig:MPC_schematic

The planar LIDAR sensor is mounted at the front center location of the vehicle. The LIDAR sensor returns the closest obstacle boundary in all radial directions of the sensor at an angular resolution . The LIDAR sensor has a maximum range past which it cannot sense any obstacles. Therefore, if the closest obstacle boundary is greater than the LIDAR radius R_{LIDAR} then the sensor returns R_{LIDAR}. The LIDAR sensor range is [0°, 180°] with 90° being the vehicle heading direction. Since for this study the AGV is driving along level ground, whether granular or rigid, the planar LIDAR sensor is sufficient. The LIDAR is assumed to have no delay and zero noise. Therefore, the LIDAR sensor can instantaneously generate a safe area polygon assembled from the returned points from the LIDAR. An overhead view of the AGV en-
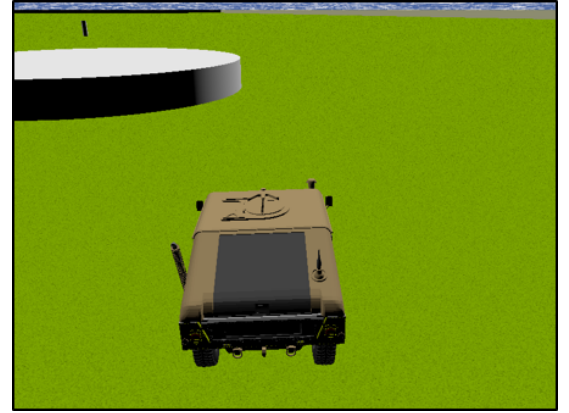
(a) 3D Visualization of LIDAR Encountering Obstacle

sub@fig:obstacle_field_3D
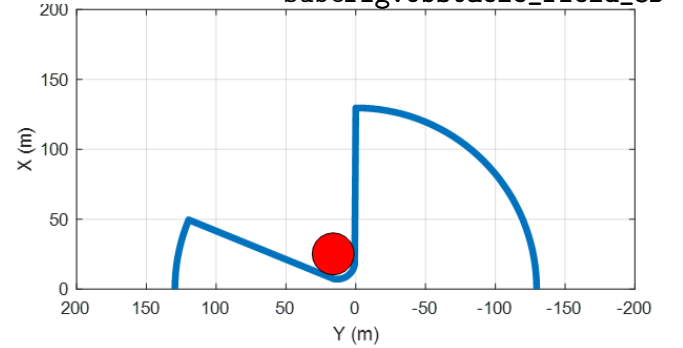
(b) LIDAR Sensed Safe Area

sub@fig:obstacle_field_LIDAR

Figure 2: Sample obstacle field and LIDAR output

fig:LIDARExample

countering an obstacle and the generated LIDAR safe area polygon are presented in Fig. 2.

fig:LIDARExample

The outputs of the MPC algorithm are the steering signals only for this simulation. As shown in Fig. 1, the MPC algorithm is made up of the internal controller vehicle model, the cost function and constraints, and the dynamic optimizer. The internal controller vehicle model predicts the future states of the AGV for a given steering sequence and is of interest in this work. For this study, the internal controller vehicle model is varied from test to test between a 2-DOF vehicle model and a 14-DOF vehicle model, detailed in further sections. The cost functions and constraints are used to formulate the optimal control problem with the equations from the vehicle model. The dynamic optimizer then solves the optimal control problem. For the purpose of this paper, exhaustive search is used to find the optimal solution to the problem since solution speed is not a primary focus of this paper, but more importantly the ability to find and execute an optimal solution.

fig:MPC_schematic

2.2 Chrono Multibody Physics Package

ss:Chrono

The physics modeling and simulation capabilities are provided by the multiphysics open-source package Chrono [2]. The core functionality of Chrono provides support for the modeling, simulation, and visualization of rigid multibody systems, with additional capabilities offered through optional modules. These modules provide support for additional classes of problems (e.g., finite element analysis and fluid-solid interaction), for modeling and simulation of specialized systems (such as ground vehicles and granular dynamics problems), or provide specialized parallel computing algorithms (multicore, GPU, and distributed) for large-scale simulations.

Chrono2016

2.2.1 Vehicle Modeling

sss:Chrono_Vehicle

Built as a Chrono extension module, Chrono::Vehicle [3] is a C++ middleware library focused on the modeling, simulation, and visualization of ground vehicles. Chrono::Vehicle provides a collection of templates for various topologies of both wheeled and tracked vehicle subsystems, as well as support for modeling of rigid, flexible, and granular terrain, support for closed-loop and interactive driver models, and run-time and off-line visualization of simulation results.

ChronoVehicle_TR

Modeling of vehicle systems is done in a modular fashion, with a vehicle defined as an assembly of instances of various subsystems (suspension, steering, driveline, etc.). Flexibility in modeling is provided by adopting a template-based design. In Chrono::Vehicle, templates are parameterized models that define a particular implementation of a vehicle subsystem. As such, a template defines the basic modeling elements (bodies, joints, force elements), imposes the subsystem topology, prescribes the design parameters, and implements the common functionality for a given type of subsystem (e.g., suspension) particularized to a specific template (e.g., double wishbone). Finally, an instantiation of such a template is obtained by specifying the template parameters (hardpoints, joint directions, inertial properties, contact material properties, etc.) for a concrete vehicle (e.g., the HMMWV front suspension).

For wheeled vehicle systems, templates are provided for the following subsystems: *suspension* (double wishbone, reduced double wishbone using distance constraints, multi-link, solid-axle, McPhearson strut, semi-trailing arm); *steering* (Pitman arm, rack-and-pinion); *driveline* (2WD and 4WD shaft-based using specialized Chrono modeling elements, simplified kinematic driveline); *wheel* (simply a carrier for additional mass and inertia appended to the suspension's spindle body); *brake*

(simple model using a constant torque modulated by the driver braking input).

In addition, Chrono::Vehicle offers a variety of tire models and associated templates, ranging from rigid tires, to empirical and semi-empirical models (such as Pacejka and Fiala), to fully deformable tires modeled with finite elements (using either an Absolute Nodal Coordinate Formulation or a co-rotational formulation). Driver inputs (steering, throttle, and braking) are provided from a *driver* subsystem with available options in ChronoVehicle including both open-loop (interactive or data-driven) and closed-loop (e.g., path-following based on PID controllers).

2.2.2 Granular Mechanics
sss:GranMech

In this work, the focus is on modeling and simulating the terrain and the tire-terrain interaction using high-fidelity, fully-resolved granular dynamics simulations, employing the so-called Discrete element Method (DEM). Meaningful mobility simulations require large enough terrain patches and small enough particle dimensions that result in DEM problems involving frictional contact with millions of degrees of freedom.

Unlike continuum-based deformable terrain modeling approaches, DEM treats all component particles separately, as distinct entities, by maintaining and advancing in time their states while taking into account pair-wise interaction forces due to frictional contact. Broadly speaking, computational methods for DEM at this scale can be categorized into two classes: penalty-based (also known as a compliant-body approach; denoted here by DEM-P) and complementarity-based (also known as a rigid-body approach; denoted here by DEM-C). While differing in the underlying formulation employed for modeling and generating the normal and tangential forces at the contact interface, and thus leading to different mathematical models and different problem sizes, both methods rely crucially on efficient methods for proximity calculation. This common algorithmic step provides a complete geometric characterization of the interaction between neighboring bodies, taking into account the current system state and specification of the contact shapes associated with all interacting bodies.

The DEM-C class of methods for granular dynamics fully embraces the rigid body assumption and formulates the frictional contact problem by imposing non-penetration conditions which result in unilateral constraints between each pair of interacting shapes. The derivation begins by defining a so-called *gap function* Φ_i which describes the separation between the two shapes involved in a potential contact i in the current active contact set. Then, a complementarity condition is imposed stating that either the distance between the two shapes is greater than zero, in which case the normal force is zero, or vice-versa; i.e., if the distance is zero, the contact force is nonzero. Introducing the Coulomb friction model via the principle of maximum dissipation [4], the problem can be formulated as a Differential Variational Inequality problem which can be converted to a cone-complementarity problem. This is further transformed into a quadratic optimization problem with conic constraints which can then be solved using projected iterative optimization schemes. See [5] for additional details on the DEM-C formulation implemented in Chrono.

Penalty methods begin with a relaxation of the rigid body assumption [6]. A regularization approach, DEM-P assumes local body deformation at the contact point. Employing the finite element method to characterize this deformation would incur a stiff computational cost. Instead, an approximation is employed, using information generated during the collision detection stage of the solution, and the local body deformation is related to the depth of inter-penetration between two otherwise rigid contact shapes. In order to apply re-

sults from Hertz contact theory, valid for sphere-sphere interactions, the contact shapes are further approximated by their local radius of curvature at the contact point [7]. This approach yields a general methodology for computing the normal and tangential forces at the contact point. For granular dynamics via DEM-P, the equations of motion need not be changed. Indeed, normal and tangential contact forces are treated as any external forces and directly factored in the momentum balance. For details on the specific DEM-P implementation in Chrono, see [8]. In this work, we employed the DEM-P capabilities in Chrono, leveraging the multi-core, OpenMP-based parallelization features offered by the Chrono::Parallel module.

3 TECHNICAL APPROACH AND METHODOLOGY

s:methodology

3.1 Full-Vehicle Multibody Model

ss:FullVehicleModel

The model to be controlled (the *plant*) is a full-vehicle Chrono::Vehicle model of an HMMWV, which includes multi-body subsystems for the suspensions, steering, driveline, and powertrain, and is available in the Chrono package.

This vehicle model (see Fig. 3) has a curb weight of $2,550$ kg. It includes independent front and rear double wishbone suspensions and a Pitman arm steering mechanism. The shock absorber and coil spring, mounted between the lower control arm and the chassis, are modeled with Chrono nonlinear force elements and include the effects of bump stops.

The AWD driveline is modeled using Chrono shaft elements and includes three power splitting elements (a central differential and front/rear differentials), as well as conical gears connected through 1-dimensional shaft elements which carry rotational inertia. The powertrain is also modeled using 1-dimensional shaft elements and includes models for a thermal engine specified through
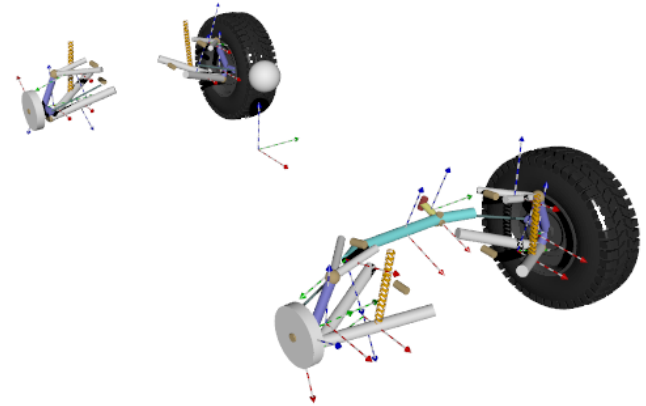

Figure 3: Full-vehicle HMMWV multibody model.

fig:hmmwv

speed-torque maps for power and engine losses, a torque converter specified via maps for the capacity factor and the torque ratio, and an automatic transmission gearbox with three forward gears and a single reverse gear. The connection between powertrain and driveline is a force-displacement interface at the driveshaft (with torque applied from the powertrain and angular velocity provided by the driveline).

For mobility studies on deformable terrain, provided that the tire inflation pressure is comparable or larger than the average ground pressure, according to the postulate by Wong [9] the tire can be considered in a so-called *rigid regime*. As such, tire deformation can be ignored and the vehicle's tires modeled using rigid contact shapes. The HMMWV tire model used here is thus represented by a cylinder with a radius of 0.47 m (18.5 in) and a width of 0.254 m (10 in).

3.2 Relocating Granular Patch

ss:Patch

Due to the large-scale nature of the simulations in this study, generating granular particles scattered across the whole obstacle field to simulate granular terrain is both computationally exhausting and unreasonable. The computational times to complete
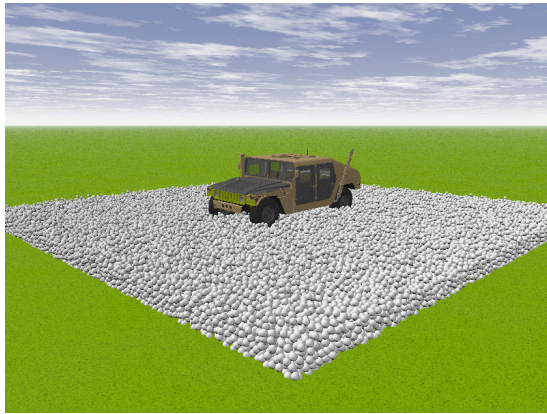
Figure 4: Relocating Granular Patch that follows the vehicle

fig:granPatch

a simulation of this sort of scale would be too large to justify the completion of this sort of study. Instead, a mechanism has been developed for this study to address the issue of scale when simulating a ground vehicle traversing over a large granular terrain. Consider an AGV on a large granular terrain of 100 by 100 meters. Since we are primarily interested in the behavior of the vehicle on the terrain and not specifically the terrain behavior itself, we assume only a small patch of granular terrain underneath and around the vehicle actually has a significant effect on vehicle behavior and performance. This idea promoted the development of a relocating granular patch used for this study to allow a vehicle to traverse granular terrain over a large-scale area without the need to generate particles everywhere throughout the terrain area.

This mechanism allows a user to generate granular particles within a specified distance of the vehicle's CoG. Figure 4 presents the patch of granular terrain underneath the Chrono HMMWV that will allow follow the HMMWV. The particles are contained within four rigid walls to prevent particles from escaping the desired terrain area. As the vehicle moves across the terrain, this granular patch maintains granular terrain underneath the vehicle by consistently relocating particles as the

become too far away from the vehicle. When the vehicle CoG comes within a certain distance of any of the walls, a band of particles from the opposite end of the granular patch are relocated past the closest wall and all of the walls are shifted in that direction. Each of these relocation steps keeps the vehicle on top of granular terrain at all times. Depending on the vehicle, this granular patch can be resized for both computationally efficiency and to guarantee the vehicle maintains a reasonable distance from the walls to prevent any edge effects. This newly developed method of simulating granular terrain for AGV's is omnidirectional in the ground plane, allowing the vehicle to move in any direction while the terrain patch relocates and responds to that movement. This method of granular terrain mobility allows the user to specify parameters of the particles and thus allows for simulation of a vehicle over a largely customizable flat terrain.

For our simulations, the granular patch was maintained at a size of roughly 6.6 by 6.6 meters. This number was assigned as two times the largest dimension of the vehicle, which in the case of the HMMWV is 3.3 m (in length). The dimensions of the patch are not constant, however, since the patch expands in the direction of relocation by two times the largest particle radius every time the advancing wall is shifted. This is done in order to avoid particle overlap, since the relocated particles are moved to a position that is shifted one largest particle radius ahead of the particles adjacent to the advancing wall. After relocation, the walls of the granular patch are given a recovery velocity such that the granular patch regains its original dimensions in 0.1 seconds. This recovery time should be small relative to the duration of the simulations, and in general it will also depend on the velocity of the vehicle, since the granular patch should completely recover its dimensions between subsequent relocations.

Within the granular patch, the granular terrain

was modeled by $55,931$ uniform spherical particles, with a micro-scale inter-particle sliding friction coefficient of $\mu = 0.8$, and particle diameter of 0.1 m. Previous studies [10] have shown that a randomly packed assembly of as few as $3,000$ - $30,000$ uniform spheres will exhibit macro-scale bulk granular material yield behavior (due to inter-particle sliding) that closely matches the Lade-Duncan yield surface, which is a well-established yield criterion in the field of geomechanics, where the macro-scale friction angle ϕ for the bulk granular material can be determined as a function of the inter-particle friction coefficient μ.

Referring to Fig. 10 of [10], a randomly packed assembly of uniform spheres with an inter-particle friction coefficient of $\mu = 0.8$ will exhibit macro-scale yield behavior corresponding to a bulk granular material with a macro-scale friction angle between roughly $35° \leq \phi \leq 40°$ if particle rotation is allowed (6 DOF particles), or with a macro-scale friction angle between roughly $65° \leq \phi \leq 70°$ if particle rotation is prohibited (3 DOF particles). Since the granular patch used in our simulations contains more than $50,000$ uniform spheres, we can reliably conclude that our granular patch is accurately modeling the yield behavior of a true granular material on the macro-scale: either with a macro-scale friction angle of $35° - 40°$ if particle rotation is allowed, which is typical of a wide range of dry natural and crushed sands [11]; or with a macro-scale friction angle of $65° - 70°$ if particle rotation is prohibited, which is typical of crushed or fragmented rock, such as railway track ballast [12].

In this first draft of our paper, we only include simulation results for the granular material model corresponding to a macro-scale or bulk material friction angle of $65° - 70°$ (using 3 DOF particles), which essentially models a field of fragmented rock. In the final draft of this paper, we will also include simulation results for the granular material model corresponding to a macro-scale bulk friction angle

of $35° - 40°$ (using 6 DOF particles), which models dry sand. Thus, in the final draft of this paper, we will compare the MPC algorithm performance on both fragmented rock and dry sand, as well as on rigid terrain.

We note that in the case of the HMMWV, the vehicle tire width is equal to only approximately 2.5 particle diameters in the granular patch. This is less than ideal. However, a more ideal value of 10 particle diameters per tire width would increase the number of particles in the granular patch to more than 3 million, which would result in prohibitively slow simulations, particularly for events corresponding to physical time durations on the order of 10 seconds or more.

3.3 Chrono Multibody Physics Package

The physics modeling and simulation capabilities are provided by the multiphysics open-source package Chrono [2]. The core functionality of Chrono provides support for the modeling, simulation, and visualization of rigid multibody systems, with additional capabilities offered through optional modules. These modules provide support for additional classes of problems (e.g., finite element analysis and fluid-solid interaction), for modeling and simulation of specialized systems (such as ground vehicles and granular dynamics problems), or provide specialized parallel computing algorithms (multi-core, GPU, and distributed) for large-scale simulations.

3.4 Implemented MPC LIDAR Based Local Obstacle Avoidance

The MPC controller as formulated in [1] is used for this study. The cost function and constraints need to be specified to avoid collisions with obstacles and guarantee vehicle dynamical safety. The optimal control problem solved at each MPC time step is comprised of the following set of equations:

$$J = s_T + wd \qquad \text{e:MPCCost} \tag{1}$$

$$\dot{\xi} = v\left[\xi\left(t\right), \zeta\left(t\right)\right] \qquad \text{e:State\_ODE} \tag{2}$$

$$\xi\left(0\right) = \xi_0 \qquad \text{e:InitialStates} \tag{3}$$

$$\tilde{S}\left[x\left(t\right), y\left(t\right)\right] \leq 0 \qquad \text{e:SafeArea} \tag{4}$$

$$\left|\delta_f\left(t\right)\right| \leq \tilde{\delta}_{f,max}\left(U_0\right) \qquad \text{e:SteerLimit} \tag{5}$$

$$\left|\varsigma_f\left(t\right)\right| \leq \varsigma_{f,max} \qquad \text{e:SteerRateLimit} \tag{6}$$

$$t \in \left[0, T_P\right] \qquad \text{e:TimeDomain} \tag{7}$$

Equation (1) e:MPCCost defines the cost function for this optimal control problem. This equation is a soft requirement which defines how the separate path possibilities are weighed against each other and how to determine which path is actually optimal. The cost function is comprised of two terms defined by the following

$$s_T = \sqrt{\left[x_G - x\left(T_P\right)\right]^2 + \left[y_G - y\left(T_P\right)\right]^2} \qquad \text{e:DistanceCost} \tag{8}$$

$$d = \int_0^{T_G} \left|\varsigma\left(t\right)\right| dt \qquad \text{e:TurningCost} \tag{9}$$

s_T seeks to minimize the distance between the prediction end location and the target position. A prediction path that predicts the vehicle at the closest location to the target will have the smaller s_T term. The second term d aims to minimize the change in steering angle so that smoother, straighter paths are more favorable than windy paths.

Equations (2-7) e:TimeDomain e:State_ODE are the constraint equations for this optimal control problem which represent hard requirements for vehicle safety and avoiding collisions. Any paths that violate these constraints are not considered safe paths and are eliminated as potential options in this prediction window. Equation (2) e:State_ODE defines a set of differential equations that describe the internal controller vehicle model. These equations are presented further in the paper or left for formulation in references. Equation (3) e:InitialStates

presents the initial states needed to solve Eq. (2) e:State_ for potential paths.

Equation (4) e:SafeArea defines a safe area polygon. All points along paths found from Eqs. (2)-(3) must fall inside of this safe area polygon. This safe area is constructed from LIDAR points. An additional safety buffer is added to account for vehicle size and prevent corners of the vehicle from colliding with an obstacle.

Equation (5) e:SteerLimit imposes a limit on maximum steering angle for the vehicle based on vehicle speed. This value is obtained from a lookup table which can be generated either experimentally or from simulation. Equation (6) e:SteerRateLimit imposes a maximum limit on steering rate. Equation (7) e:TimeDomain defines the time limits over which this optimal control problem is solved.

Equation (2) e:State_ODE as noted above refers to an analytical vehicle model expressed as a set of differential equations. This is how the controller is able to predict vehicle performance within the prediction horizon. The accuracy of the internal vehicle controller model should directly influence the driven vehicle's controlled performance. If the internal vehicle controller model poorly predicts a vehicle's response to inputs from the driver or the environment, then these deficiencies will be witnessed when attempting to control the driven vehicle. In the case of this study, an internal vehicle controller model that poorly represents the driven vehicle may predict that a specified steering sequence will navigate the driven vehicle around an approaching obstacle, but due to this descrepancy the driven vehicle may not turn quickly enough and collide with the obstacle. However, using an internal vehicle controller model that is highly complex may provide accurate trajectory and vehicle response predictions, but the time required to solve an optimal control problem with this complicated set of differential equations is much higher than using a simpler internal vehicle controller model. Since the eventual goal is physical implementation of this

controller, an ideal controller would not just accurately predict vehicle responses but also do it quick enough to insure vehicle safety. Therefore for this study the driven vehicle that will be controlled is a HMMWV developed in Chrono. This vehicle will be controlled using two separately developed controllers. The first controller uses a simple 2 DOF vehicle model to predict the Chrono HMMWV trajectory for different series of steering sequences and is presented in detail in Section 3.5.1. The second controller uses a complex 14 DOF vehicle model to predict vehicle states for different series of steering sequences. Once again, this study will test each of these controller's abilities to successfully navigate the driven Chrono HMMWV vehicle through two obstacle fields on rigid flat terrain and then granular terrain. The driven Chrono HMMWV vehicle is presented in detail in Section 3.1. Exhaustive search space is used to solve the optimal control problem in each time step since the goal of this study is to analyze the vehicle's ability to be successfully navigated through an obstacle field and not how quickly the problem can be solved. A sample visualization of the different predicted trajectories from the 2 DOF model is presented in Fig. 5. A point in polygon algorithm is used to determine which trajectories remain inside of the safe area polygon visualized in Fig. ?? and therefore should be compared to the other possibilities using Eq. (1).

3.5 Internal Controller Vehicle Models

The vehicle models embedded in the MPC are simplifications of the full, multi-body based, Chrono wheeled vehicle model which is being controlled. We consider two such models, providing different levels of fidelity, as described below.

3.5.1 Two DOF Vehicle Model

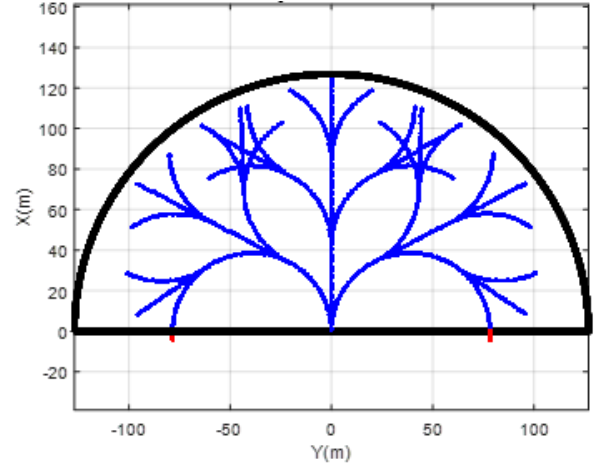The standard vehicle model used in newly developed MPC obstacle avoidance algorithms such

Figure 5: Potential Paths predicted by 2 DOF Internal Vehicle Controller Model

as [1] is the 2-DOF vehicle model. These models normally either assume constant cornering stiffness or the nonlinear Pacejka Magic Formula Tire Model [?] to predict the ground tire interaction forces. For this study and due to the availability of experimental data, the Pacejka Magic Formula is used to predict tire forces in the vehicle models.

A visual representation of the 2-DOF model can be found in Fig. 6. The two DOF model is described by the following first-order ordinary differential equations:

$$\dot{V} = (F_{y,f} + F_{y,r})/M - U_0 r \tag{10}$$

$$\dot{r} = (F_{y,f} - F_{y,r})/I_{zz} \tag{11}$$

$$\dot{\psi} = r \tag{12}$$

$$\dot{x} = U_0 \cos\psi - (V + L_f r)\sin\psi \tag{13}$$

$$\dot{y} = U_0 \sin\psi + (V + L_f r)\cos\psi, \tag{14}$$

where $F_{y,f}$ and $F_{y,r}$ are the lateral tire forces at the front and rear axles, respectively. U_0 and V are the longitudinal speed and lateral speed of the vehicle in the vehicles coordinate frame. ψ is the yaw angle and r is the yaw rate. (x, y) represent the front center location of the vehicle expressed in global coordinates. M is vehicle mass, I_{zz} is the
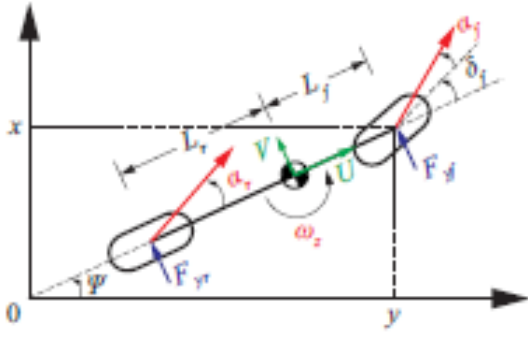
Figure 6: Two DOF Vehicle Model [1] ModelFidelity2016 fig:2DOF

Test Number	Terrain Type	Controller Vehicle Model
1	Rigid	2DOF
2	Rigid	14DOF
3	Granular	2DOF
4	Granular	14DOF

Table 1: Individual Simulation Test Information t:TestMatrix

moment of inertia of the vehicle, L_f is the distance from the front axle to the vehicle CoG, and L_r is the distance from the rear axle to the vehicle CoG.

3.5.2   Fourteen DOF Vehicle Model
sss:14DOFModel

A fourteen DOF model is often used in studies such as these to test the obstacle avoidance controller with a higher fidelity vehicle model [1, 13]. A benefit of using the fourteen DOF in the controller is the models ability to predict tire liftoff and account for dynamic effects from suspension systems. For this paper then it is appropriate to also compare performance of the local obstacle avoidance controller running an internal fourteen DOF on rigid terrain versus granular terrain.

The fourteen DOF vehicle model consists of one sprung mass connected above four unsprung masses [14]. The sprung mass is allowed to roll, pitch, and yaw while also displacing laterally, vertically, and longitudinally. This sprung mass contributes six DOF to the model. Each of the four wheels are allowed to bounce vertically and rotate about the wheel horizontal axis. The front two wheels are also free to steer. Each wheel then contributes two DOF to the fourteen DOF model. The equations used for this model as well as their developments can be found in [14].

3.6   Evaluation Metrics
ss:Metrics

Five evaluation metrics will be used to compare one test performance to the other. First, all test runs will be compared based on the time to reach the target T_{target}. Tests on the same terrain can be compared with this metric to determine which controller leads the vehicle to the target point quickest. Second, the closest distance the vehicle reaches to any obstacle d_{min} will be measured. A controller that accurately predicts vehicle performance should allow the vehicle get much closer to obstacles. Third, the control effort will be calculated and compared between test cases. Fourth, the max lateral acceleration of the vehicle will be determined. Finally, the average lateral acceleration will be determined from the test cases. These five evaluation metrics provide a logical method for comparing one test case to another whether two test cases are on different terrain, have different analytical controller models, or both.

3.7   Numerical Simulation Setup
ss:Setup

Simulations on both rigid and granular terrain were compared to understand how the controller performs on non-ideal surfaces. The two internal controller vehicle models to be studied in these tests are the previously described two DOF and fourteen DOF vehicle models. Aside from changing the internal controller vehicle model from study to study, the rest of the controller will remain the
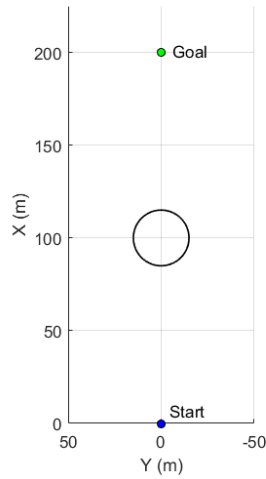
Figure 7: Obstacle Field 1   fig:Obst1

	x	y	Radius
Target Location	200.0	0.0	-
Obstacle 1	100.0	0.0	15.0

Table 2: Obstacle Field 1 Summary   t:Obst1Summary

same. Referring to Table t:TestMatrix, Tests 1 and 2 will be compared to understand how model fidelity influences controller performance on rigid flat terrain. Tests 3 and 4 will be compared to again understand the role of model fidelity in the MPC controller on granular terrain. Tests 1 and 3 will be compared to understand how the same controller performs differently on granular terrain as opposed to rigid flat terrain. Similar comparisons will be made between Tests 2 and 4. Each of the tests will consist of one run on two different obstacle fields created to target the controllers ability to navigate the vehicle through certain obstacle combinations.

For this paper two obstacle fields were generated. The first contains one large circular obstacle located along the initial heading of the vehicle. The target position is located a large distance then behind the single obstacle. Figure fig:Obst1 presents this obstacle field. The goal of this test is to analyze the
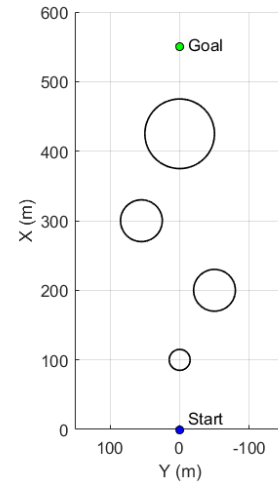

Figure 8: Obstacle Field 2   fig:Obst2

	x	y	Radius
Target Location	550.0	0.0	-
Obstacle 1	100.0	0.0	15.0
Obstacle 2	200.0	-50.0	30.0
Obstacle 3	300.0	55.0	30.0
Obstacle 4	425.0	0.0	50.0

Table 3: Obstacle Field 2 Summary   t:Obst2Summary

performance of the vehicle and controller around a single obstacle.

The second obstacle field contains four circular obstacles of varying sizes placed in the vehicles initial heading direction. The performance of the vehicle on this obstacle field should allow for understanding of how the controller and vehicle navigate around multiple obstacles in a more realistic scenario. Refer to Fig. 8.

4 SIMULATION RESULTS

s:results

This section summarizes the results of the four tests listed in Table 1.

The trajectories for the four performed tests are presented in Fig. 9a on Obstacle Field 1 and Fig. 10a on Obstacle Field 2 and their associated steering commands generated by the controller are presented in Fig. 9b and 10b. Just from looking at the trajectories of the vehicles, several observations can be made. The controlled vehicle in each test successfully maneuvers around the single obstacle in Obstacle Field 1. From this we can see as has been proven in [1] that even though the 2DOF vehicle model lacks the complexity and fidelity of the 14DOF model, it can still safely navigate a vehicle successfully through an obstacle field while moving at a non-extreme speed. The evaluation metrics for each test as defined in Section 3.6 are tabulated for the runs on each obstacle field. The evaluation metrics for the runs on Obstacle Field 1 are presented in Table 4 and for Obstacle Field 2 in Table 5.

Comparing the results of Test 1 and Test 2, we are able to examine the performance differences that occur when a 2DOF internal vehicle model is used within the controller to control the Chrono vehicle as opposed to the higher fidelity 14DOF internal vehicle model used in the controller in Test 2. On both Obstacle Field 1 and 2, the controllers that use the 14DOF internal vehicle model to predict vehicle states guides the Chrono vehicle to the
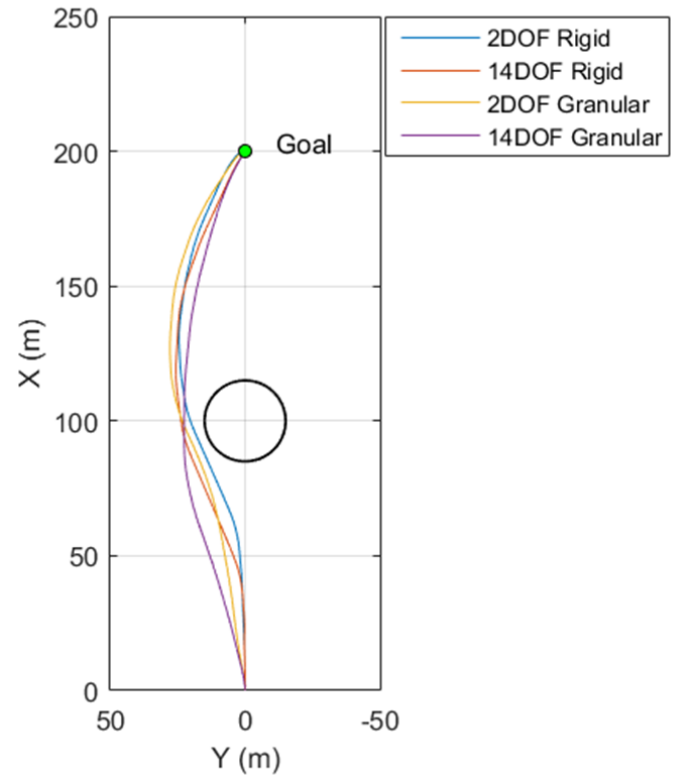
(a) Trajectories from Tests on Obstacle Field 1.

sub@fig:ObstacleField1Trajectories

(b) Steering Commands on Obstacle Field 1.
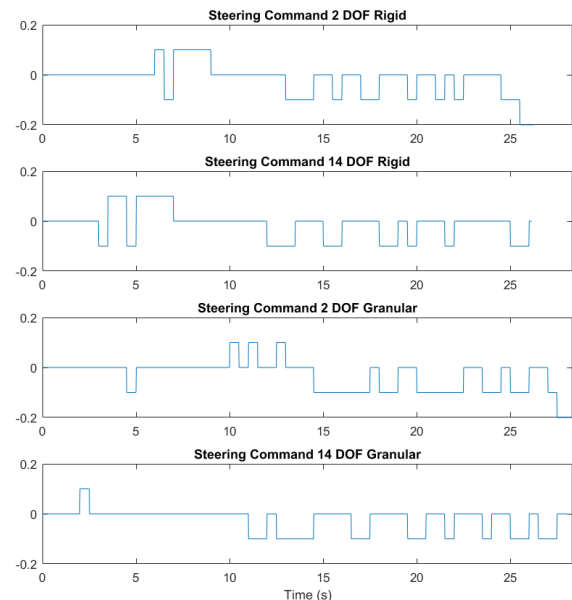
sub@fig:SteeringCommandsField1

Figure 9: Trajectories and Steering Data for Obstacle Field 1

fig:Obst1TestData

Test Number	1	2	3	4
Controller Model	2DOF	14DOF	2DOF	14DOF
Terrain	Rigid	Rigid	Granular	Granular
Time to Target (s)	26.67	26.15	28.32	28.03
Minimum Obstacle Distance (m)	0.897	5.462	3.491	4.721
Controller Effort	0.0340	0.0340	0.0340	0.0306
Max Lateral Acceleration (m/s$\hat{2}$)	2.78	1.57	2.47	2.33
Average Lateral Acceleration (m/s$\hat{2}$)	0.54	0.51	0.55	0.46

Table 4: Test Evaluation Metrics Summary on Obstacle Field 1
t:EvalMetricsObst1

Test Number	1	2	3	4
Controller Model	2DOF	14DOF	2DOF	14DOF
Terrain	Rigid	Rigid	Granular	Granular
Time to Target (s)	73.85	71.55	76.64	74.70
Minimum Obstacle Distance (m)	0.331	2.599	1.083	1.152
Controller Effort	0.0510	0.0680	0.0714	0.0612
Max Lateral Acceleration (m/s^2)	2.92	2.51	2.55	2.45
Average Lateral Acceleration (m/s^2)	0.41	0.43	0.53	0.58

Table 5: Test Evaluation Metrics Summary on Obstacle Field 2
t:EvalMetricsObst2
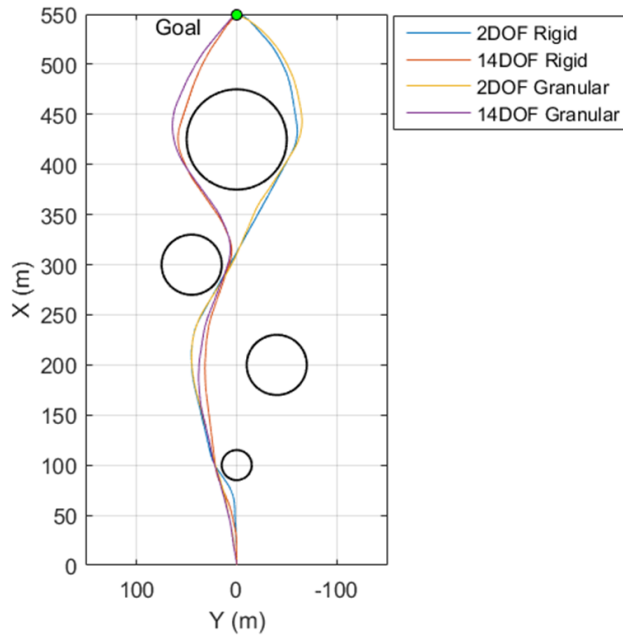
(a) Trajectories from Tests on Obstacle Field 2.
sub@fig:ObstacleField2Trajectories
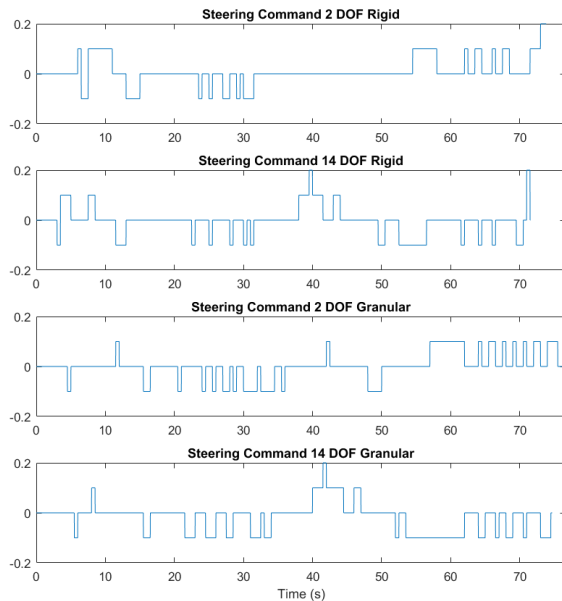
(b) Steering Commands on Obstacle Field 2.
sub@fig:SteeringCommandsField2

Figure 10: Trajectories and Steering Data for Obstacle Field 2

fig:Obst2TestData

goal quicker than the controllers with the internal 2DOF vehicle model. However, in each of these instances the time difference is slim. At most in these tests a controller using the 14DOF internal vehicle reaches the target 2.2 seconds faster than the 2DOF controller tests. So in this regard the 14DOF controllers perform marginally better than the 2DOF controllers. One area the 2DOF controller model of Test 1 performs better than the 14DOF model of Test 2 is in the minimum Obstacle Distance metric. In all the cases, the controllers with the 2DOF internal vehicle model guided the vehicle closer to the obstacles than the controllers with the 14DOF models. This is a desirable characteristic in that the 2DOF controllers are taking more advantage of the controlled vehicle's dynamic capabilities when navgiating around obstacles. Comparing the controller effort between Tests 1 and 2, on Obstacle Field 1 the controller effort is actually the same. The 2DOF controller does input more command changes than the 14DOF controller. On Obstacle Field 2, the 14DOF controller of Test 2 actually has a higher controller effort value than the 2DOF controller by 0.0170. This may however be due to the controller's decision to move left around the last obstacle instead of continueing straight around the right side of the obstacle as the 2DOF controller commands. Finally looking at the maximum and average lateral accelerations between test 1 and test 2, regarding both of these metrics the 14DOF controller performs better than the 2DOF controller on rigid terrain. Overall looking at all these metrics, on rigid terrain the 14DOF controller performs marginally better than the 2DOF controller. However considering the 14DOF takes much longer to run and the fact that realtime implementation of a 14DOF model would be less feasible, the 2DOF is suitable for use in an MPC local obstacle avoidance controller for a vehicle on rigid ground terrain traveling at non-extreme speeds. The performance drop is slight switching to the 2DOF vehicle model, but

can still safely navigate the vehicle around an obstacle field to an end goal. These results support the findings and conlusions of [1] on a different AGV.

ModelFidelity2016

The same set of comparisons are made between the 2DOF controller and the 14DOF controller but now on granular terrain in Tests 3 and 4. Similar to on rigid ground, the 14DOF controller navigates the Chrono vehicle to the specified end goal quicker than the 2DOF controller at most by 1.94 seconds. Again though, this time difference is marginal so even though the 14DOF controller performs better than the 2DOF controller regarding time to target, this does not mean at all that the 2DOF controller performs poorly. On Obstacle Field 1 and Obstacle Field 2, the 2DOF controller guides the vehicle closer to obstacles on granular terrain than the 14DOF controllers. The 14DOF controller has a lower controller effort value than the compared 2DOF controller on granular terrain in Tests 3 and 4. Finally looking at the maximum and average lateral accelerations between Tests 3 and 4, on Obstacle Field 1 the 2DOF has a higher maximum lateral acceleration and average lateral acceleration. On Obstacle Field 2 the 2DOF controller results in a lower maximum lateral acceleration and average lateral acceleration than the 14DOF controller of test 4 on granular terrain. Overall looking at the previously mentioned metrics, the 14DOF controller again performs marginally better than the 2DOF controller on granular terrain. Even though the 2DOF and 14DOF internal vehicle models were derived using rigid ground assumptions, they are still capable of successfully navigating the Chrono vehicle through an obstacle field safely on certain granuler media. The same conclusion from this comparison can be made as from comparing Tests 1 and 2. Though vehicle performance marginally drops when using the 2DOF controller, realistically the software benefits of using the 2DOF controller outweigh the slight performance drop seen by this study at non-extreme vehicle speeds.

By comparing Tests 2 and 4, observations are made about the difference between a vehicle operating on rigid ground versus granular terrain when the controller is held constant. In this case, the controller used is the 14DOF controller so we can analyze performance differences between navigating on rigid ground versus granular terrain. In all cases the time to target is lower on rigid ground tests than on granular tests we will ignore that evaluation metric when making the comparison between Tests 2 and 4. In Test 4, the vehicle navigates much closer to any obstacle than in Test 2 on rigid ground. On granular terrain though, the controller effort is lower than on rigid ground. Comparing the lateral acceleration metrics of Tests 2 and 4 yield no discernable conclusions since neither is significantly nor consistently larger than the other in either of the tests. Comparing Tests 1 and 3 yields similar conclusions as comparing Tests 2 and 4. On rigid ground, the 2DOF controller does a better job of approaching the obstacles more closely. The controller effort is also lower in Test 1 on rigid ground than on granular terrain in Test 3.

Just from looking at the lateral accelerations, we see the forces the vehicle experiences from driving on granular terrain can be much different than forces on simple rigid ground. Even examining Figs. 9a and 10a, the vehicle navigating on granular terrain does not turn as sharply for a given steering command as the vehicle does on rigid ground terrain. To really understand the differing behavior between a vehicle driving on rigid terrain to a vehicle driving on granular terrain, a parametric study should be performed analyzing the vehicle driving on a variety of granular terrain with different granular parameters.

fig:ObstacleObstacle14Raged2trajesctories

5   CONCLUSIONS

s:conclusion

In this study, using the multibody physics API Chrono a simulation has been developed of a

HMMWV driving through a user specified obstacle field towards a defined target location. Within this simulation, a MPC LIDAR based local obstacle avoidance controller has been implemented to navigate the vehicle around obstacles as it encounters them. The controller itself uses a simplified analytical vehicle model to predict the actual controlled Chrono vehicle states within a finite prediction horizon in order to determine the optimal path and steering sequence forward from the current vehicle state. A novel method of simulating granular terrain for this large obstacle field was developed and implemented for this study. Two seperate MPC Algorithms were developed, one that uses a 2DOF vehicle model to predict Chrono vehicle states and a 14DOF model to do the same. These two controllers were used to navigate a Chrono HMMWV through two obstacle courses on both rigid terrain and then on granular terrain. The results were compared to understand what if any improvements need to be made to the MPC LIDAR based local obstacle avoidance controller to successfully control a vehicle on granular terrain.

As in [1], the controller with the 14DOF internal vehicle model performs marginally better than the controller with the 2DOF internal vehicle model in all situations. However, tests with the 2DOF controller prove that this controller can still successfully navigate a vehicle through an obstacle field when the vehicle is moving at non-extreme speeds. Using the 2DOF controller also allows for faster calculation of optimal steering sequences which is required for eventual realtime implementation. Both of the controllers navigated the vehicle worse on granular terrain than on rigid ground terrain, but this is expected since the internal vehicle controller models were derived using rigid ground assumptions. This study also highlights the complexities introoduced to vehicle modeling when the terrain is no longer rigid ground. Looking at the vehicle trajectories and lateral accelerations on granular terrain, there are clear differences in

tire ground interactions when the terrain is now granular. The terrain granular parameters affect the turning characteristics of the vehicle, acceleration abilities, and overall vehicle dynamic performance which is not accounted for with the currently used 2DOF and 14DOF analytical vehicle models.

The results of this study are promising. Since the 2DOF controller is able to navigate the Chrono vehicle on this study's granualr terrain, then there is some small set of granular terrain on which a 2DOF model is sufficient for predicting vehicle performance well enough to guide the vehicle successfully and safely to a target point. However, these results also emphasize the need for future research and studies relating to vehicle simulation on granular terrain. This same sort of study should be performed parametrically on a comprehensive set of different granular terrains to understand the difference between vehicle performance on rigid ground and granular terrain. From there, a new intermediate analytical model should be research and developed that is not as complex as the 14DOF model but does take into account granuler parameters such as the friction angle.

Acknowledgments

REFERENCES

[1] J. Liu, P. Jayakumar, J. L. Stein, and T. Ersal. A study on model fidelity for model predictive control-based obstacle avoidance in high-speed autonomous ground vehicles. *Vehicle System Dynamics*, 2016.

[2] A. Tasora, R. Serban, H. Mazhar, A. Pazouki, D. Melanz, J. Fleischmann, M. Taylor, H. Sugiyama, and D. Negrut. Chrono: An open source multi-physics dynamics engine. In T. Kozubek, editor, *High Performance Computing in Science and Engineering – Lecture Notes in Computer Science*, pages 19–49. Springer, 2016.

[3] R. Serban and D. Negrut. Chrono::Vehicle – Template-Based Ground Vehicle Modeling and Simulation. Technical Report TR-2016-10: `http://sbel.wisc.edu/documents/TR-2016-10.pdf`, Simulation-Based Engineering Laboratory, University of Wisconsin-Madison, 2016.

[4] J.J. Moreau. On unilateral constraints, friction and plasticity. In *New variational techniques in mathematical physics*, pages 171–322. Springer, 2011.

[5] D. Negrut and R. Serban. Posing Multibody Dynamics with Friction and Contact as a Differential Algebraic Inclusion Problem. Technical Report TR-2016-12: `http://sbel.wisc.edu/documents/TR-2016-12.pdf`, Simulation-Based Engineering Laboratory, University of Wisconsin-Madison, 2016.

[6] P. Cundall. A computer model for simulating progressive large-scale movements in block rock mechanics. In *Proceedings of the International Symposium on Rock Mechanics. Nancy, France*, 1971.

[7] K.L. Johnson. *Contact mechanics*. Cambridge University Press, 1987.

[8] J. Fleischmann, R. Serban, D. Negrut, and P. Jayakumar. On the importance of displacement history in soft-body contact models. *Journal of Computational and Nonlinear Dynamics*, 11(4):044502–1–5, 2016.

[9] J. Y. Wong. *Theory of ground vehicles*. J. Wiley, New York, N.Y., 2nd edition, 1993.

[10] J. A. Fleischmann, M. E. Plesha, and W. J. Drugan. Determination of yield surfaces for isotropic non-cohesive particulate materials by the discrete element method. *Geotechnical and Geological Engineering*, 32(4):1081–1100, 2014.

[11] G.-C. Cho, J. Dodds, and J. C. Santamarina. Particle shape effects on packing density, stiffness, and strength: Natural and crushed sands. *Journal of Geotechnical and Geoenvironmental Engineering*, 132(5):591–602, 2006.

[12] B. Indraratna, D. Ionescu, and H. D. Christie. Shear behavior of railway ballast based on large-scale triaxial tests. *Journal of Geotechnical and Geoenvironmental Engineering*, 124(5):439–449, 1998.

[13] J. Liu, P. Jayakumar, J. L. Stein, T. Ersal, and J. L. Overholt. The role of model fidelity in model predictive control based hazard avoidance in unmanned ground vehicles using lidar sensors. *Dynamic Systems and Control Conference*, 2013.

[14] T. Shim and C. Ghike. Understanding the limitations of different vehicle models for roll dynamics studies. *Vehicle System Dynamics*, 2007.